

# Generalization of World Models under Environmental Variability for Vision-based Quadrotor Navigation

Luca Zanatta\*, Grzegorz Malczyk\*, and Kostas Alexis  
 Norwegian University of Science and Technology  
 \*Equal contribution

**Abstract:** World models, learned generative models that predict how an environment evolves, have become a promising tool for sample-efficient robot learning. Yet how robust they are to environmental variability remains poorly understood. To address this, we conduct a systematic study using vision-based quadrotor navigation as a testbed problem, training DreamerV3-based world models under varying levels of environmental randomness and evaluating them across all levels through cross-environment validation, spanning both Self-Supervised Learning (SSL) pretraining and Reinforcement Learning (RL) fine-tuning. We then deploy all world models and associated navigation policies on a real quadrotor in unseen environments, including an open-loop run where the model receives just 2.5 s of real sensory input before all sensors are cut off, leaving the system to navigate entirely in imagination over a 12 m traverse. Our results show that world model robustness during SSL pretraining is a strong predictor of sim-to-real transfer: every model that generalized well in cross-environment SSL validation deployed successfully in the real world, passing through gaps as narrow as 0.67 m, whereas the model that dominated simulation policy evaluation failed on the real platform. We further identify (a) the discrete latent size and (b) the training-sequence length as the dominant factors governing world model quality.

**Keywords:** World Models, Vision-Based Navigation, Reinforcement Learning

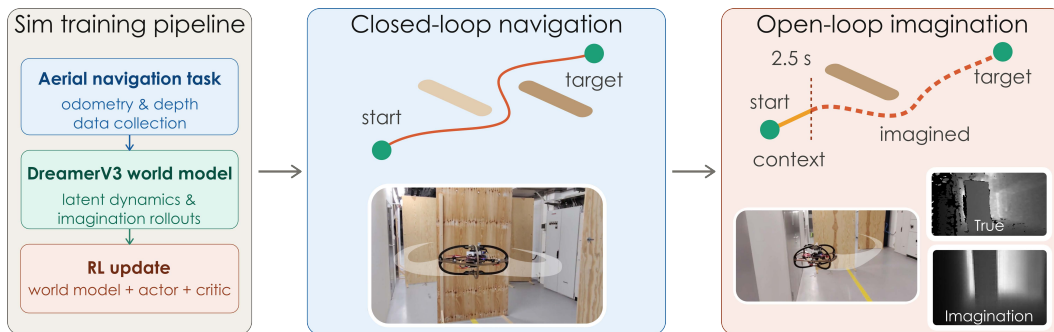


Figure 1: From simulation to real-world closed- and open-loop deployment.

## 1 Introduction

Advances in embodied AI emphasize predictive representation learning, where the agent learns an internal model of how the world evolves under its actions. According to this paradigm, Model-Based Reinforcement Learning (MBRL) leverages a learned dynamics model, referred to as the world model, in order to synthesize future experience through latent imagination as opposed to exclusively relying on computationally expensive interaction with the environment [1, 2]. By enabling agents to internally predict future trajectories, world models offer a pathway toward improved sample efficiency, long-horizon reasoning, and scalable decision making in high-dimensional problems [3, 4, 5, 6, 7, 8]. In fact, beyond policy optimization alone, world models demonstrate potential

to serve as a more general computational primitive for embodied intelligence, supporting state estimation, trajectory prediction, and self-supervised representation learning across diverse robotic systems [9, 10, 11, 12, 13].

Despite progress, it remains unclear whether learned predictive representations consistently generalize across different environments. Yet this is essential for training world model-based navigation policies [12]. Existing approaches typically evaluate within relatively fixed settings, implicitly assuming that training and deployment environments are highly similar [3, 4, 5, 6] or even require exact digital twins of the target environment [14]. While these methods yield interesting results, their achieved control performance does not necessarily imply that the learned predictive model captures transferable and generalizable structure about the environment. This limitation is particularly important for vision-based navigation of agile robotic systems such as flying systems. In such tasks, predictive performance may degrade significantly due to environmental variability (structure, obstacle configuration, light conditions, texture). The problem is made even more demanding by the sudden viewpoint changes inherent to agile flight dynamics.

While recent works have explored applying world models to the autonomous navigation of aerial robots [14, 15, 16], an important limitation of the current state-of-the-art remains: the lack of systematic analysis regarding environmental variability and generalization. In [14], the authors train separate world models for specific individual racing tracks and validate deployment in a hardware-in-the-loop setup, without investigating transfer across environments. The work in [15] demonstrates sim-to-real transfer across two scenarios but mitigates the visual reality gap through specialized preprocessing of the onboard observations into binary gate masks before training the world model. These works highlight that understanding how world model quality degrades, or holds, as environmental randomness increases is a prerequisite for reliable sim-to-real transfer, yet no systematic analysis has been conducted in the context of vision-based autonomous navigation.

To address this gap, we consider the problem of depth image-based collision-free navigation with a quadrotor as our target task and conduct a comprehensive robustness analysis regarding how DreamerV3-based world model [5] generalizes and responds to environment variability. As opposed to training against specific environments, we explicitly train and evaluate across environments of varying randomness without any preprocessing of the onboard sensor stream. We adopt DreamerV3 specifically because its reconstruction objective enables direct evaluation of imagined observations against real sensor readings. We vary the degree of environmental randomness across both the SSL pretraining phase and RL fine-tuning, evaluating generalization through systematic cross-environment validation, and conclude with a real-world deployment in pure world model imagination, as shown in Figure 1. Our investigation proceeds in four stages: SSL pretraining, hyperparameter analysis, RL fine-tuning, and real-world deployment operating purely within world model imagination.

## 1.1 Contributions

Taken together, our contributions characterize world model robustness from simulation to the real world. We first study how environmental randomness during SSL pretraining shapes learned representations by cross-evaluating models trained across varying randomness levels. To our knowledge, this is the first systematic characterization of world model sensitivity to domain shift in vision-based quadrotor flight. Second, a structured hyperparameter search over the SSL phase identifies the configurations that produce robust world models, yielding practical guidelines for training DreamerV3-based systems. We next apply this cross-environment protocol to RL fine-tuning, where randomness comes only through the parameters of the low-level controller, isolating its impact on policy robustness. Finally, we evaluate all trained models on a real quadrotor in unseen environments through a closed-loop deployment, and an open-loop run in which the model hallucinates future depth and state from its own dynamics after just 2.5 s of real input and flies on imagination alone. The method is open-sourced in <https://github.com/ntnu-arl/world-model-nav-generalization>.

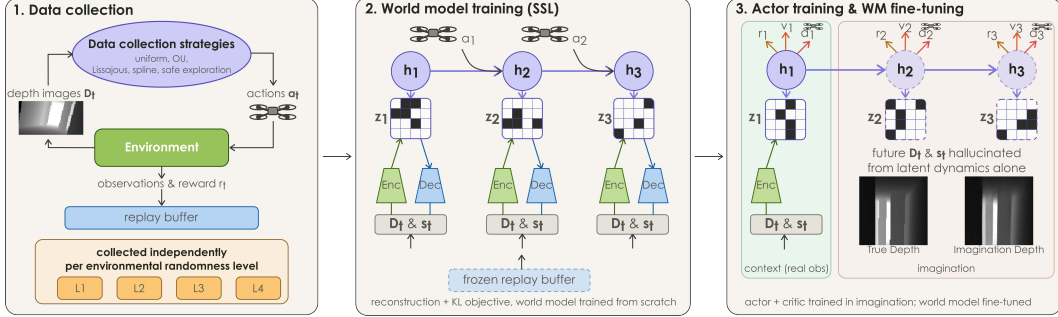


Figure 2: **Method overview.** First, the data is collected per environmental randomness level. Next, the DreamerV3 world model is trained by self-supervised reconstruction. Finally, an actor and critic are trained in imagination with world-model fine-tuning: after a real-observation context (green), the model rolls out in pure imagination (orange), hallucinating future observations.

## 2 Problem Formulation

This work investigates the limits and potential of MBRL through predictive world models for autonomous collision-free 3D navigation in unknown environments using onboard depth perception. Let us denote the inertial frame as  $\mathcal{I}$ , the body-fixed frame as  $\mathcal{B}$ . At time  $t$ , the robot state is  $\mathbf{s}_t = [\mathbf{p}_t, \mathbf{v}_t, \mathbf{R}_t, \boldsymbol{\omega}_t]$ , where  $\mathbf{p}_t = [p_{x,t}, p_{y,t}, p_{z,t}]^\top$ , is the position defined in  $\mathcal{I}$ ,  $\mathbf{v}_t = [v_x, v_y, v_z]^\top$  is the linear velocity expressed in  $\mathcal{I}$ ,  $\mathbf{R}_t \in \text{SO}(3)$  is the rotation matrix from  $\mathcal{I}$  to  $\mathcal{B}$ , and  $\boldsymbol{\omega}_t = [\omega_x, \omega_y, \omega_z]^\top$  is the angular velocity in  $\mathcal{B}$ . The robot additionally perceives its surroundings through a depth image  $\mathbf{D}_t$ , which together with  $\mathbf{s}_t$  constitutes the full onboard observation available to the agent at each timestep.

Given a goal position  $\mathbf{p}_{\text{goal}}$  in  $\mathcal{I}$ , the current state  $\mathbf{s}_t$ , and the depth image  $\mathbf{D}_t$ , the objective of this work is to learn a control policy  $\pi$  that outputs velocity commands  $\mathbf{a}_t = [a_{v_x}, a_{v_y}, a_{v_z}, a_{\omega_z}]^\top$  in  $\mathcal{B}$ , comprising a 3D linear velocity command and a yaw rate, such that the robot reaches  $\mathbf{p}_{\text{goal}}$  while avoiding collisions with obstacles. To keep motion within the camera field of view, we constrain the action space: the lateral velocity is fixed to  $a_{v_y} = 0$ , and the longitudinal and vertical commands  $a_{v_x}, a_{v_z}$  are projected onto the maximum inclination angle. Unlike the dominant robot-learning literature in this domain, which employs model-free RL, the focus here is explicitly on MBRL.

## 3 Method

The method comprises three stages, illustrated in Figure 2: (a) data collection under varying levels of environmental randomness (Section 3.1), (b) SSL pretraining of DreamerV3 world models with hyperparameter optimization (Section 3.2), and (c) RL fine-tuning of the best world model per randomness level (Section 3.3). All stages are conducted in the AerialGym simulator [17].

### 3.1 Data collection

To investigate world model robustness to domain shift, we define four levels of environmental randomness of increasing complexity within a simulated indoor environment of  $16 \times 7 \times 7$  m containing five cuboid obstacles of size  $0.1 \times 1.2 \times 7$  m. All levels share the same environment geometry; randomness is introduced through how obstacles, spawn, and goal positions are configured at episode initialization. Each level  $L_i$  defines an environment configuration, and we denote the world model trained on data collected in  $L_i$ , together with its fine-tuned policy, as  $\text{WM}_i$  throughout the paper. In the least randomized setting, L1, obstacles are in a fixed configuration with only the spawn and goal positions sampled uniformly at each episode. L2 introduces structured diversity by selecting at each episode from five distinct fixed obstacle configurations, one of which coincides with the L1 placement. L3 increases diversity further by drawing obstacle positions from a Sobol quasi-random sequence [18], which ensures low-discrepancy coverage of the environment space, that is, obstacles are distributed more uniformly across the room than pure random sampling would achieve. Lastly,

L4 is the maximally stochastic setting, with obstacles, spawn, and goal positions all sampled uniformly and independently at every episode (see Section A). Since no pre-trained policy is available at the beginning of training, trajectories for SSL are collected using a set of exploration strategies. High-frequency strategies generate temporally diverse action sequences that cover the action space: uniform random sampling, Ornstein-Uhlenbeck (OU) noise [19], Lissajous curves, and a pseudo-spline smooth random walk. As a low-frequency strategy, we use a reactive depth-based controller we term *safe exploration*, which steers the quadrotor by comparing mean depth across left, center, and right horizontal image sectors, applying corrective yaw commands when the forward sector approaches a proximity threshold. All these strategies yield trajectories spanning qualitatively distinct flight regimes, from highly stochastic motion to geometrically structured traversals. Data is collected independently for each level  $L_i$ . For clarity, we summarize: WM1 is trained in a fixed-layout environment (L1), WM2 on episodes drawn from five fixed layouts (L2), WM3 on Sobol-distributed obstacle placements (L3), and WM4 on fully i.i.d. uniform placements (L4).

### 3.2 World model training (SSL)

We build on DreamerV3 [6], which learns a world model of the environment’s dynamics and optimizes a policy entirely within latent imagination. At each step, the agent receives a depth image  $\mathbf{D}_t$  and proprioceptive state  $\mathbf{s}_t$ , and outputs an action  $\mathbf{a}_t$ . The world model is a Recurrent State-Space Model (RSSM) with a deterministic recurrent state  $\mathbf{h}_t$  and a categorical stochastic state  $\mathbf{z}_t$ :

$$\begin{aligned} \text{recurrent model: } \mathbf{h}_t &= f_\phi(\mathbf{h}_{t-1}, \mathbf{z}_{t-1}, \mathbf{a}_{t-1}), \\ \text{encoder: } \mathbf{z}_t &\sim q_\phi(\mathbf{z}_t \mid \mathbf{h}_t, \mathbf{D}_t, \mathbf{s}_t), \\ \text{dynamics predictor: } \hat{\mathbf{z}}_t &\sim p_\phi(\hat{\mathbf{z}}_t \mid \mathbf{h}_t), \\ \text{decoder: } (\hat{\mathbf{D}}_t, \hat{\mathbf{s}}_t) &= g_\phi(\mathbf{h}_t, \mathbf{z}_t), \\ \text{reward predictor: } \hat{r}_t &\sim p_\phi(\hat{r}_t \mid \mathbf{h}_t, \mathbf{z}_t), \end{aligned}$$

where  $\phi$  denotes the parameters of the world model. The latent state  $\{\mathbf{h}_t, \mathbf{z}_t\}$  encodes both memory and uncertainty, and the decoder grounds it in perceptual content, enabling imagined observations to be compared directly against real state and depth readings at deployment. The world model is trained to minimize a joint objective:  $\mathcal{L}_\phi = \mathcal{L}_{\text{rec}} + \mathcal{L}_{\text{rew}} + \beta \mathcal{L}_{\text{KL}}$  where  $\mathcal{L}_{\text{rec}}$  reconstructs  $\mathbf{D}_t$  and  $\mathbf{s}_t$ ,  $\mathcal{L}_{\text{rew}}$  predicts the reward, and  $\mathcal{L}_{\text{KL}}$  regularizes the stochastic state by aligning the encoder  $q_\phi$  and dynamics predictor  $p_\phi$ , as illustrated in the “World model training” stage of Figure 2.

For each randomness level, a dedicated world model WM $i$  is trained on the collected trajectories via SSL by minimizing the loss  $\mathcal{L}_\phi$ . To identify robust configurations, a sequential (coordinate-wise) search is conducted independently per randomness level over four hyperparameters. The deterministic state size  $d_{\text{det}}$  sets the capacity of the Gated Recurrent Unit (GRU) hidden state in the RSSM, controlling how much temporal context the model can retain across timesteps. The Multi-Layer Perceptron (MLP) hidden size  $d_{\text{hid}}$  controls the width of the transition and representation networks, governing the expressiveness of the learned mappings between latent states. The discrete latent size  $d_{\text{disc}}$  sets the number of classes per categorical variable in the stochastic state  $\mathbf{z}_t$ , determining the resolution of the discrete bottleneck through which uncertainty is encoded. Finally, the batch length  $L_{\text{batch}}$  controls the length of trajectory sequences sampled during training, affecting how much temporal context is available for the RSSM to learn long-range dependencies. The search is conducted sequentially: we jointly tune the RSSM size  $d_{\text{det}} \times d_{\text{hid}}$ , then the batch length  $L_{\text{batch}}$ , subsequently the discrete latent size  $d_{\text{disc}}$ , and also verify that the resulting configuration is stable across random seeds. Each candidate is evaluated by its reconstruction loss on held-out trajectories from the same level. This yields one best configuration per randomness level, which is then evaluated on all other levels, in both the context and imagination phases, to form the cross-environment validation matrix.

### 3.3 Actor training & WM fine-tuning

The best-performing world model from each randomness level is fine-tuned using RL entirely within latent imagination, as shown in the third stage of Figure 2. The actor policy  $\pi_\theta$  is optimized to

maximize the expected discounted cumulative reward:  $J(\pi_\theta) = \mathbb{E}_{\pi_\theta} \left[ \sum_{t=0}^T \gamma^t r_t \right]$  where  $\theta$  denotes the policy parameters,  $T$  is the episode length,  $r_t$  denotes the reward at time  $t$ , and  $\gamma \in (0, 1)$  is the discount factor. The reward function combines a proximity term with a time-efficiency bonus:  $r_t = 2 e^{-\|d_t\|^2} + 2 e^{-0.008 \|d_t\|^2} + [\text{win}] \cdot (T - t_{\text{win}})$  where  $d_t$  is the Euclidean distance to the goal at time  $t$ , and a win is declared when  $\|d_t\| < 0.5$  m. The first two exponential terms provide a dense guidance signal at both short and long ranges, respectively, while the final term rewards reaching the goal with remaining time steps, encouraging efficient navigation. Crash and explicit win bonuses are set to zero, so the agent is shaped entirely through proximity and time efficiency.

The actor unrolls trajectories through the RSSM and the critic estimates the value function  $V_\psi(\mathbf{h}_t, \mathbf{z}_t)$  along the imagined rollouts. The actor is trained by backpropagating gradients directly through the imagined trajectory using Exponential Moving Average (EMA)-normalized targets:  $\mathcal{L}_{\text{actor}} = -\mathbb{E}_{\tau \sim \pi_\theta} \left[ \sum_{t=0}^{H-1} w_t \cdot \frac{V_t^\lambda - \mu}{\sigma} \right]$ , where  $H$  is the imagination horizon,  $V_t^\lambda$  is the  $\lambda$ -return,  $w_t$  are importance weights, and  $\mu$  and  $\sigma$  are running EMA statistics of the return distribution. To introduce control-level uncertainty during fine-tuning, the parameters of the flying vehicle controller [20], used as the low-level dynamics model, are randomized at each episode, isolating the effect of dynamics mismatch on policy robustness independently of visual or obstacle-placement variability [21, 22]. The cross-environment evaluation protocol from the SSL phase is applied identically here, testing each policy across all levels of randomness in both the context and imagination phases.

## 4 Results

Our evaluation follows three stages. We first examine self-supervised pretraining, analyzing hyperparameter sensitivity and cross-environment reconstruction quality in Section 4.1. We then evaluate RL fine-tuning in terms of policy performance and imagination fidelity in Section 4.2, concluding by the deployment of all models on a real quadrotor in unseen environments, in both closed-loop and open-loop imagination in Section 4.3.

### 4.1 Self-Supervised Pretraining Analysis

The sequential sweep is shown in Figure 3. In every cell, the best configuration (colored) converges to a clearly lower loss than the remaining candidates (grey), and this margin holds across all four environments. The winning configurations uniformly favor large RSSM capacity ( $d_{\text{det}}=d_{\text{hid}}=1024$ ) and long batch sequences ( $L_{\text{batch}}=64$ ), with  $d_{\text{disc}}=64$  for L1/L2 and  $d_{\text{disc}}=32$  for L3/L4, suggesting a mild preference for smaller discrete bottlenecks at higher environmental randomness. A single configuration generalizes well across randomness levels: world model quality is governed far more by architectural and training choices than by the environment it is trained in, so the same configuration can be reused across environments without per-environment re-tuning. Subsequently, we report the relative impact of each hyperparameter on evaluation loss,  $\Delta = \frac{\ell_{\text{worst}} - \ell_{\text{best}}}{\ell_{\text{worst}}}$ , across all four environments in Figure 4. The discrete latent size  $d_{\text{disc}}$  and batch length  $L_{\text{batch}}$  are consistently the most influential parameters, but in different ways:  $L_{\text{batch}}$  contributes a stable  $\Delta \approx 35\%$  across environments, whereas  $d_{\text{disc}}$  is both the strongest and the most variable, ranging from  $\approx 35\%$  to  $\approx 50\%$  and peaking at higher randomness. The RSSM sizes  $d_{\text{det}}$  and  $d_{\text{hid}}$  have a moderate effect ( $\Delta \approx 20\%$ ), while seed variance is negligible ( $\Delta < 5\%$ ), confirming that the differences reflect architectural sensitivity rather than training noise. The world model performance is driven dominantly by the capacity of the stochastic state and the training sequence length.

Figure 5 presents Mean Squared Error (MSE) and Structural Similarity Index Measure (SSIM) for each world model evaluated across all environments, split into the context phase ( $t < 1$  s, conditioned on real observations) and the imagination phase ( $t \geq 1$  s, purely hallucinated). We report both metrics throughout, as they capture complementary aspects of reconstruction quality (see Section C for a qualitative illustration). During context, all models achieve low MSE and high SSIM on the diagonal, confirming that each world model fits its training distribution well. Performance degrades off-diagonal, particularly for WM1 and WM2 when evaluated on higher-randomness en-

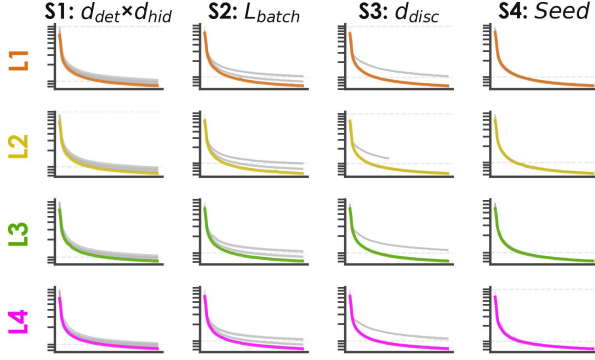


Figure 3: Hyperparameter sweep results: each cell shows all runs per environment (grey) with the best configuration highlighted. Stages S1–S4 sweep RSSM size, batch length, discrete latent size, and seed, respectively, in sequence. For more details, please refer to Section B.

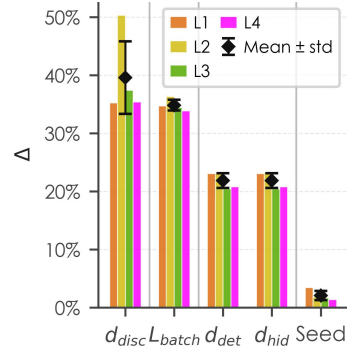


Figure 4: Hyperparameter sensitivity across environments. The relative loss gap  $\Delta$  between the worst and best value of each hyperparameter, per environment (L1-L4).

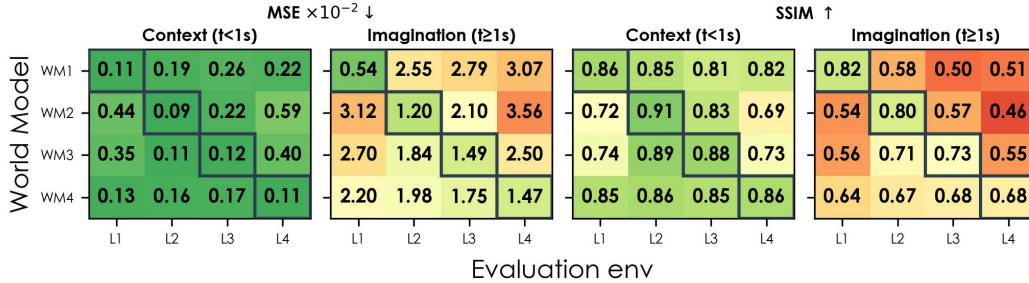


Figure 5: Cross-environment validation heatmap (MSE $\downarrow$  / SSIM $\uparrow$ ) reports reconstruction quality for world model WM $i$  evaluated on environment L $j$ , split into context and imagination.

vironments, reflecting the limited diversity of their training data. Moreover, world models trained in more structured environments have better reconstruction in the imagination phase. This behavior can be seen in the diagonal, where WM1 and WM2 perform better than WM3 and WM4.

## 4.2 Actor Training & World Model finetuning

In Table 1, we report the win, crash, and timeout rates for each world model policy, evaluated across all training environments and one Out-Of-Distribution (OOD) layout (a randomly sampled 10-cuboid environment). A win is defined as reaching the target proximity, a crash as any contact with the environment, and a timeout otherwise. Within the training distribution, WM1 achieves the highest win rate on its native environment (99.5%). However, its performance degrades sharply as evaluation randomness increases, with the crash rate rising from 0.5% to 44.5% in the OOD case. This reflects the limited diversity of the L1 training data: the policy overfits to the fixed obstacle structure rather than learning a general avoidance strategy. In contrast, WM3, trained on Sobol-sampled obstacle placements, is the most consistent, with win rates above 89.5% within the training distribution and exceeding 72.0% on the challenging OOD layout. Notably, WM4 does not outperform WM3 despite its more diverse training environment, suggesting that maximal stochasticity introduces variability that hampers policy convergence during RL fine-tuning. Across all models, timeout rates are negligible, indicating that failures are exclusively collisions rather than navigation stagnation.

We report reconstruction metrics for the RL-fine-tuned world models evaluated across all layouts, split into context and imagination phases in Figure 6. Overall reconstruction quality is lower than in the SSL phase (Figure 5), as expected: the checkpoint is selected by win rate rather than reconstruction loss, so the world model is optimized for policy return rather than perceptual fidelity. Even so, context-phase MSE and SSIM remain consistent across all models and layouts, confirming that the RSSM still assimilates real observations regardless of fine-tuning objective. Degradation is instead

Table 1: RL cross-environment policy evaluation. Win rate ( $\uparrow$ ), crash rate ( $\downarrow$ ), and timeout rate ( $\downarrow$ ) in %. Diagonal entries (in-distribution) are underlined.

	Win Rate $\uparrow$					Crash Rate $\downarrow$					Timeout Rate $\downarrow$				
	L1	L2	L3	L4	OOD	L1	L2	L3	L4	OOD	L1	L2	L3	L4	OOD
WM1	<u>99.5</u>	89.5	72.5	75.0	54.5	<u>0.5</u>	10.5	27.0	25.0	44.5	<u>0.0</u>	0.0	0.5	0.0	1.0
WM2	88.0	<u>88.5</u>	87.5	90.0	55.5	12.0	<u>11.5</u>	12.5	10.0	44.5	0.0	<u>0.0</u>	0.0	0.0	0.0
WM3	97.0	96.5	<u>92.5</u>	89.5	<b>72.0</b>	3.0	3.5	<u>7.5</u>	10.5	<b>27.0</b>	0.0	0.0	<u>0.0</u>	0.0	1.0
WM4	91.5	95.0	95.0	<u>88.0</u>	67.0	8.5	5.0	5.0	<u>11.5</u>	32.5	0.0	0.0	0.0	<u>0.5</u>	0.5

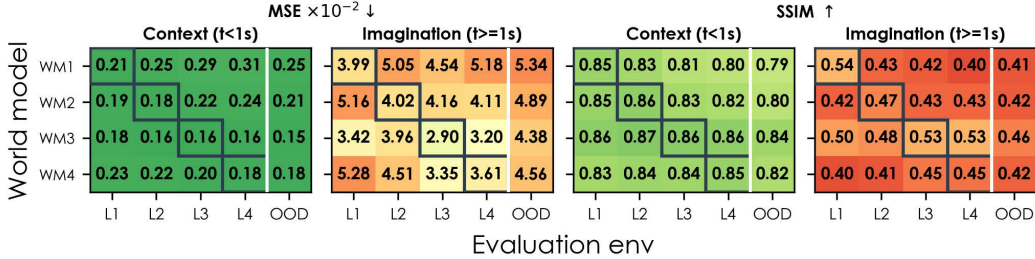


Figure 6: RL imagination cross-environment validation (MSE $\downarrow$  / SSIM $\uparrow$ ) reports reconstruction for world model WM $i$  evaluated on environment L $j$ , split into context and imagination.

concentrated in the imagination phase, where the policy-optimized dynamics accumulate errors over the open-loop horizon. In Section D, we visualize this temporal degradation on a representative rollout. Notably, WM1 shows the sharpest drop in SSIM under OOD evaluation, reinforcing that low training randomness limits generalization across both policy and world model dimensions.

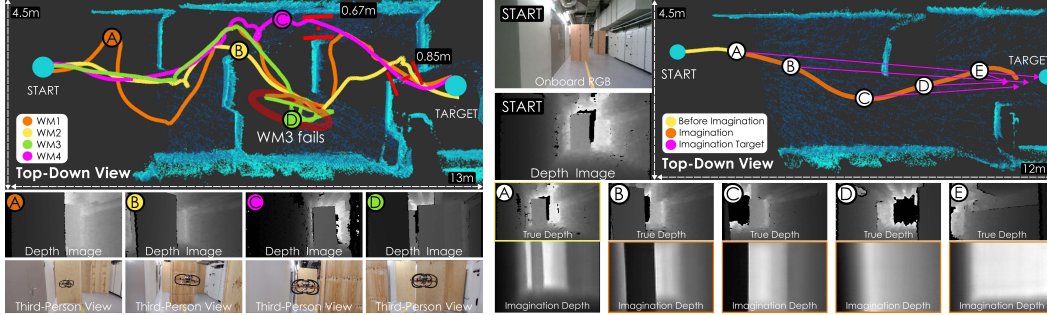
Taken together, Section 4.1 and Section 4.2 reveal a consistent trend: world models that generalize well across environments during SSL pretraining tend to produce more robust policies after RL fine-tuning. WM4 is the most generalizable world model at the SSL stage, yet WM3 yields the strongest policy, suggesting that intermediate training randomness strikes the best balance between representational diversity and the stability required for policy optimization.

### 4.3 Real-World Deployment

We deploy all trained models on a real quadrotor in a previously unseen indoor environment, under two conditions: closed-loop, with real depth and state observations fed continuously, and open-loop, in which the model flies entirely on imagined observations after a brief context window.

**Closed-loop** In Figure 7a, we present the executed trajectories in a cluttered corridor. The environment is narrower than the one used in simulation, and it consists of seven planar panels (versus five cuboids in simulation), which serve as obstacles. WM1, WM2, and WM4 traverse successfully the full 13 m from start to target, passing through gaps as narrow as 0.67 m and 0.85 m, only marginally wider than the 0.5 m quadrotor body. WM3 enters instead a looping behavior from which it does not recover (marker **D**), though it remains collision-free. This result is the opposite of what the simulation predicts: WM3 produced the most robust policy in cross-environment RL evaluation. All models maintain stable performance throughout the runs, indicating that their learned representations tolerate the noise of real depth streams. These results validate the sim-to-real transfer of the trained world models and suggest that both low and high training randomness, embodied here by WM1/WM2 and WM4, respectively, can yield deployable policies, while intermediate randomness does not always guarantee the best real-world outcome.

**Open-loop imagination** Finally, Figure 7b demonstrates a more demanding setting. With a brief context window of 2.5 s, from marker **A** onward, the model receives no further sensory input and rolls out future depth and state entirely from its latent dynamics. While the environment composed of fewer obstacles than the closed-loop experiments, the imagined trajectory traces 12 m path toward the target. As shown on insets in Figure 7b, early predictions closely match the real depth stream,



(a) Closed-loop real-world deployment. Top-down trajectories of all trained world models. Three reach the target while WM3 fails to find the path at marker D. Insets show onboard depth and third-person views.

(b) Open-loop imagination in the real world. After 2.5 s of context (yellow), all sensors are cut off (marker A), and the robot flies in imagination (orange). The target position with magenta arrows and image insets contrasts the true sensor state and depth reading with the imagined rollout.

Figure 7: Real-world deployment: closed-loop (a) and pure-imagination open-loop (b) navigation.

correctly hallucinating corridor walls and obstacle edges, while fidelity gradually degrades over longer horizons. Further real-world results are provided in Section E.

Every model that generalized well across environments during SSL pretraining transferred successfully to the real world, while the model that dominated RL simulation evaluation was not able to find the path to the target. This indicates that SSL cross-environment reconstruction quality is a more reliable predictor of real-world deployability than RL win rate, and that intermediate training randomness, while optimal in simulation, does not guarantee the best real-world outcome.

## 5 Limitations

All real-world experiments use panel-like obstacles matching those in simulation: large, planar, and easily resolved in a depth image. We do not evaluate smaller objects, which give weaker geometric cues, nor thin structures such as railings, which depth sensors capture poorly. Whether our robustness trends carry over to such cases remains open. Furthermore, reliable imagination holds only over brief horizons, as the open-loop deployment shows accurate prediction over short rollouts. At longer horizons, errors in the latent dynamics compound, and the imagined state and depth observation degrade significantly. Finally, the notion of randomness could be potentially larger as the findings characterize robustness to geometric and control-level variation primarily.

## 6 Conclusion

We present a systematic study of how world models generalize under environmental randomness in depth-based quadrotor navigation. By leveraging DreamerV3’s reconstruction objective, we directly compare imagined observations against real state and depth readings. Across SSL pretraining and RL fine-tuning, we observe a clear trend that strong cross-environment reconstruction during SSL pretraining directly translates to robust policies after RL fine-tuning and identify  $d_{\text{disc}}$  and  $L_{\text{batch}}$  as the dominant hyperparameters defining world model quality. Notably, every model that generalized well in SSL cross-environment validation transferred successfully to a real quadrotor in an unseen environment, flying through gaps as narrow as 0.67 m, whereas the model that dominated in simulation failed to navigate in a cluttered environment. This indicates that SSL reconstruction quality predicts deployability more reliably than RL win rate. The open-loop experiment showed that a world model can fly a real quadrotor through a 12 m corridor on imagination alone, without hallucinating a path into an obstacle. We hope this cross-environment validation framework provides a practical baseline for future deployable MBRL systems.

## Acknowledgments

This work was supported by the Horizon Europe Grant Agreement No. 101120732 and the Research Council of Norway under Award NO-338694. The authors are with the Department of Engineering Cybernetics, Norwegian University of Science and Technology (NTNU), Norway.

## References

- [1] D. Ha and J. Schmidhuber. Recurrent world models facilitate policy evolution. *Advances in neural information processing systems*, 31, 2018.
- [2] M. Janner, J. Fu, M. Zhang, and S. Levine. When to trust your model: Model-based policy optimization. *Advances in neural information processing systems*, 32, 2019.
- [3] D. Hafner, T. Lillicrap, I. Fischer, R. Villegas, D. Ha, H. Lee, and J. Davidson. Learning latent dynamics for planning from pixels. In *International conference on machine learning*, pages 2555–2565. PMLR, 2019.
- [4] D. Hafner, T. Lillicrap, J. Ba, and M. Norouzi. Dream to control: Learning behaviors by latent imagination. In *International Conference on Learning Representations*, 2020. URL <https://openreview.net/forum?id=S110TC4tDS>.
- [5] D. Hafner, T. P. Lillicrap, M. Norouzi, and J. Ba. Mastering atari with discrete world models. In *International Conference on Learning Representations*, 2021. URL <https://openreview.net/forum?id=0oabwyZb0u>.
- [6] D. Hafner, J. Pasukonis, J. Ba, and T. Lillicrap. Mastering diverse control tasks through world models. *Nature*, 640(8059):647–653, 2025.
- [7] E. Aljalbout, M. Krinner, A. Romero, and D. Scaramuzza. Accelerating model-based reinforcement learning with state-space world models. In *ICLR 2025 Workshop on World Models: Understanding, Modelling and Scaling*, 2025.
- [8] L. Maes, Q. L. Lidec, D. Scieur, Y. LeCun, and R. Balestriero. Leworldmodel: Stable end-to-end joint-embedding predictive architecture from pixels. *arXiv preprint arXiv:2603.19312*, 2026.
- [9] J. Schrittwieser, I. Antonoglou, T. Hubert, K. Simonyan, L. Sifre, S. Schmitt, A. Guez, E. Lockhart, D. Hassabis, T. Graepel, et al. Mastering atari, go, chess and shogi by planning with a learned model. *Nature*, 588(7839):604–609, 2020.
- [10] P. Wu, A. Escontrela, D. Hafner, P. Abbeel, and K. Goldberg. Daydreamer: World models for physical robot learning. In *Conference on robot learning*, pages 2226–2240. PMLR, 2023.
- [11] N. Hansen, H. Su, and X. Wang. Td-mpc2: Scalable, robust world models for continuous control. In *International Conference on Learning Representations*, volume 2024, pages 47376–47405, 2024.
- [12] A. Bar, G. Zhou, D. Tran, T. Darrell, and Y. LeCun. Navigation world models. In *Proceedings of the Computer Vision and Pattern Recognition Conference*, pages 15791–15801, 2025.
- [13] C. Li, A. Krause, and M. Hutter. Robotic world model: A neural network simulator for robust policy optimization in robotics. In *NeurIPS 2025 Workshop on Embodied World Models for Decision Making*, 2025. URL <https://openreview.net/forum?id=u76d3gBWCX>.
- [14] A. Romero, A. Shenai, I. Geles, E. Aljalbout, and D. Scaramuzza. Dream to fly: Model-based reinforcement learning for vision-based drone flight. *arXiv preprint arXiv:2501.14377*, 2025.

- [15] A. Verraest, S. Bahnam, R. Ferede, G. de Croon, and C. De Wagter. Skydreamer: Interpretable end-to-end vision-based drone racing with model-based reinforcement learning. *arXiv preprint arXiv:2510.14783*, 2025.
- [16] I. Geles, L. Bauersfeld, A. Romero, J. Xing, and D. Scaramuzza. Demonstrating agile flight from pixels without state estimation. In *Robotics: Science and Systems (RSS)*, 2024.
- [17] M. Kulkarni, W. Rehberg, and K. Alexis. Aerial gym simulator: A framework for highly parallelized simulation of aerial robots. *IEEE Robotics and Automation Letters*, 2025.
- [18] I. M. Sobol. Distribution of points in a cube and approximate evaluation of integrals. *USSR Computational mathematics and mathematical physics*, 7:86–112, 1967.
- [19] G. E. Uhlenbeck and L. S. Ornstein. On the theory of the brownian motion. *Physical review*, 36(5):823, 1930.
- [20] T. Lee, M. Leok, and N. H. McClamroch. Geometric tracking control of a quadrotor uav on se (3). In *49th IEEE conference on decision and control (CDC)*, pages 5420–5425. IEEE, 2010.
- [21] J. Tobin, R. Fong, A. Ray, J. Schneider, W. Zaremba, and P. Abbeel. Domain randomization for transferring deep neural networks from simulation to the real world. In *2017 IEEE/RSJ international conference on intelligent robots and systems (IROS)*, pages 23–30. IEEE, 2017.
- [22] X. B. Peng, M. Andrychowicz, W. Zaremba, and P. Abbeel. Sim-to-real transfer of robotic control with dynamics randomization. In *2018 IEEE international conference on robotics and automation (ICRA)*, pages 3803–3810. IEEE, 2018.

## Appendix

### A Design of the Environmental Randomness Levels

The choice of environmental randomness levels in Section 3.1 is important within this work, since this defines how we can measure world model generalization. In this section, we summarize the reasoning behind both the four-level progression and the use of Sobol sampling for the L3 environment.

**A four-level  $L_i$  progression.** The environmental levels should span a meaningful range of distributional diversity while keeping the number of  $L_i$  small enough that every model can be cross-evaluated against every level. With  $n$  levels, cross-environment validation requires training  $n$  world models and evaluating  $n^2$  combinations. The corresponding RL fine-tuning adds another  $n$  runs, and real-world deployment must be repeated per model. We chose four levels as we assumed that this would provide a good balance: enough resolution to observe a monotonic effect along the environmental randomness axis, while keeping the full study computationally tractable. The levels are chosen to span qualitatively distinct regimes rather than uniformly spaced points: (a) L1 fixes obstacles entirely, (b) L2 introduces categorical diversity (a small set of structured layouts), (c) L3 introduces spatial diversity with controlled spread, and (d) L4 introduces full variability (independent uniform sampling). Each level, therefore, probes a distinct property of the world model.

**Why Sobol distribution for L3 environment** The role of L3 is to provide an intermediate level of randomness between the structured L2 layouts and the maximally stochastic L4 setting. We use a Sobol quasi-random sequence [18] because uniform sampling is unbiased only in expectation. This means that in any single episode with only five obstacles, independent uniform draws can cluster in one region of the room while leaving large gaps elsewhere, producing visually degenerate configurations that might not exploit the world model’s perception in a useful way. Sobol sequences are designed to avoid this. By construction, they have low discrepancy, meaning successive draws fill the configuration space more evenly than independent uniform samples at the same sample count. L3 therefore produces obstacle layouts that are randomized across episodes and well-distributed within each episode, while L4 reverts to fully independent uniform draws and thus introduces the full distribution of clustering effects.

This separation is what makes the contrast between L3 and L4 meaningful. The difference with Sobol at L3 and i.i.d. uniform at L4 isolates the effect of additional within-episode variability, beyond well-distributed placement, and helps unravel two distinct notions that “more random” otherwise conflates: spread across the configuration space, and unpredictability across individual draws. The results in Sections 4.1 and 4.2 suggest this distinction matters: WM4 and WM3 differ in cross-environment generalization and policy stability.

### B Hyperparameter Sweep Details

We perform a sequential grid search over four stages. In S1 we jointly vary the deterministic state size  $d_{det} \in \{245, 512, 1024\}$  and the hidden size  $d_{hid} \in \{256, 512, 1024\}$  of the RSSM, fixing the remaining parameters to their defaults. The configuration with the lowest evaluation loss is carried forward to S2, where we sweep the batch sequence length  $L_{batch} \in \{16, 32, 64\}$ . S3 then sweeps the number of discrete latent categories  $d_{disc} \in \{0, 32, 64\}$ , where 0 means normal distribution, hence no categorical. Finally, S4 re-runs the best overall configuration with five different random seeds to confirm that the results are not seed-dependent. Figure 8 shows the full set of learning curves for all four environments across all stages.

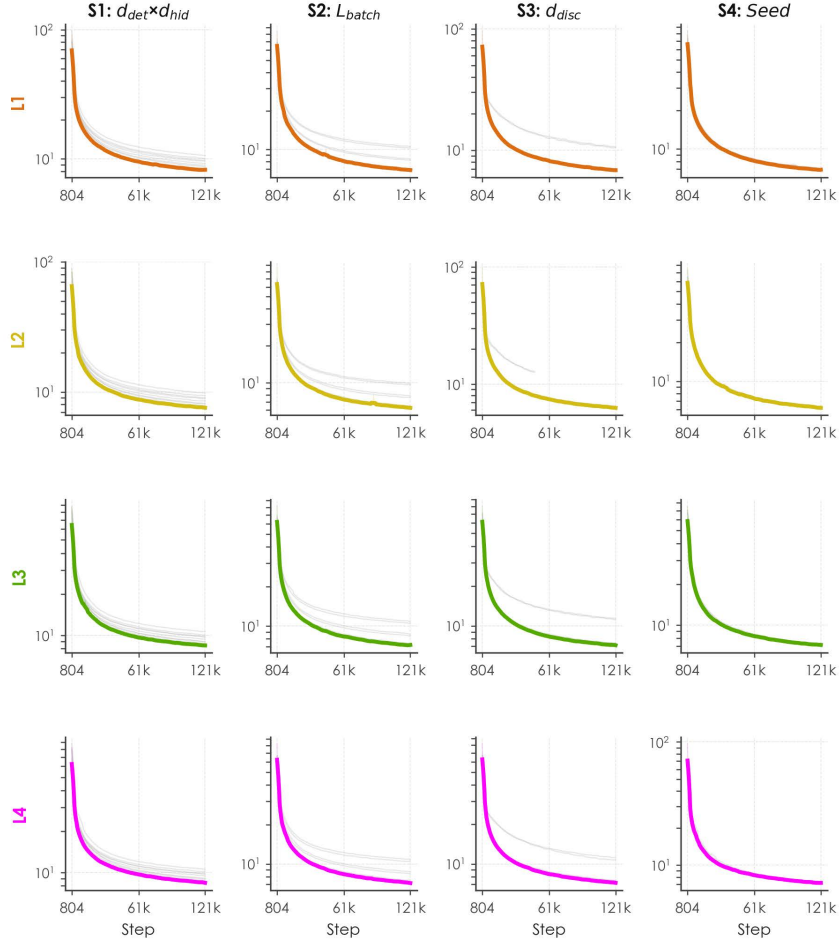


Figure 8: Hyperparameter sweep with full learning curves. Each cell shows all runs for a given environment (row) and sweep stage (column). The best configuration (lowest evaluation loss) is highlighted in the environment colour and all others are shown in grey. Loss is plotted on a log scale. S1 sweeps RSSM state size ( $d_{det} \times d_{hid}$ ), S2 batch length ( $L_{batch}$ ), S3 discrete latent size ( $d_{disc}$ ), and S4 confirms robustness across random seeds.

## C Interpreting MSE and SSIM

Throughout our evaluation, we report both MSE and SSIM, as the two metrics capture complementary aspects of reconstruction quality and do not always agree. Figure 9 illustrates this with three representative ground-truth, prediction, and difference (GT/Pred/Diff) triplets. Case (A) shows a prediction with substantial pixel-level error (high MSE) that nonetheless preserves the scene’s structure (high SSIM): the walls and obstacle edges are correctly placed, but their absolute depth values are offset. Case (B) shows a prediction that fails on both counts, missing the structure entirely and scoring poorly on both metrics. Case (C) is an accurate reconstruction, with low MSE and high SSIM. The contrast between (A) and (B) is important: MSE alone would rank both as poor, yet (A) is structurally faithful and (B) is not. We therefore report both metrics throughout, since neither alone fully characterizes prediction fidelity, and structural similarity is often the more relevant criterion for downstream aerial navigation.

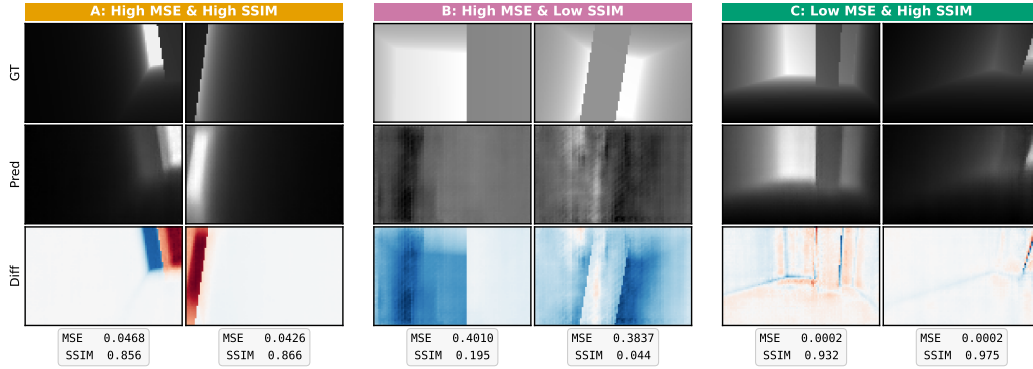


Figure 9: Qualitative illustration of MSE and SSIM as complementary reconstruction metrics. Each panel shows a GT/Pred/Diff triplet for a representative case: (A) high MSE yet high SSIM, where pixel-level errors are present but structural patterns are preserved; (B) high MSE and low SSIM, indicating both pixel-level and structural failure; (C) low MSE and high SSIM, corresponding to accurate reconstruction of both intensity and structure.

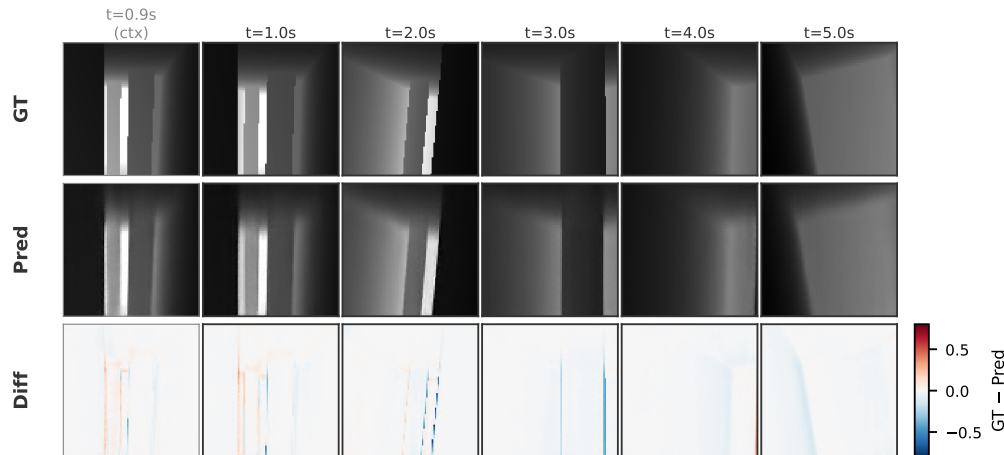


Figure 10: Temporal evolution of imagined depth observations during open-loop rollout. The last context frame ( $t = 0.9$  s) is followed by purely hallucinated predictions ( $t = 1.0 - 5.0$  s). Rows show ground-truth depth (GT), predicted depth (Pred), and their signed difference (Diff), with red indicating over-prediction and blue under-prediction. Prediction fidelity degrades gradually over the imagination horizon as latent dynamics errors accumulate.

## D Imagination Rollout Over Time

Figure 10 shows a representative open-loop rollout in simulation, comparing the ground-truth depth (GT), the world model’s prediction (Pred), and their signed difference (Diff) at successive horizons. After the final context frame ( $t = 0.9$  s), the model receives no further depth input and predicts purely from its latent dynamics. As expected, and compared to the real-world deployment, the predictions track more closely the true depth, correctly reconstructing walls and cuboids, and residual error appears mainly at cuboid edges.

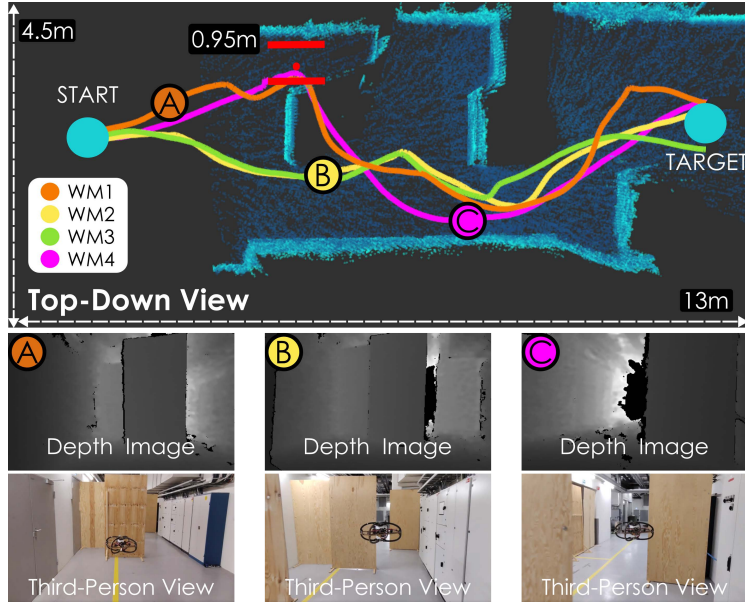


Figure 11: Closed-loop real-world deployment with 5 cuboid obstacles. Top-down trajectories of all trained world models. All trained world models successfully reach the target. Insets show onboard depth and third-person views. The red marker indicates the narrowest gap in this setting.

Table 2: Real-world evaluation. Number of successful trials out of total per condition, for two closed-loop environments and the open-loop imagination test. A timeout denotes failure to reach the target within the time limit (looping), with the flight remaining collision-free.

World model	5 panels	7 panels	Imagination
WM1	3/3	4/4	2/2
WM2	3/3	4/4	2/2
WM3	3/3	0/4 (timeout)	2/2
WM4	3/3	3/4 (1 crash)	2/2

## E Additional Real-World Deployments

To deeply assess the trained world models, we initially deploy them in an environment that is closer to the training distribution. We repeat the closed-loop deployment in a setting by populating the corridor with five panels, matching the obstacle count used in simulation, as illustrated in Figure 11. Here, all four world model policies, namely WM1, WM2, WM3, and WM4 reach the target, some passing through a gap of 0.95 m while maintaining clearance from obstacles. This demonstrates successful sim-to-real transfer while the trained policies are deployed in environments similar to the training.

In Table 2, we summarize all real-world runs across the two closed-loop environments and the open-loop imagination experiments. The 5-panel environment matches the obstacle count used in simulation. All four models reach the target in every trial. The denser 7-panel environment reproduces the pattern reported in the main text: WM1 and WM2 succeed in all runs, WM4 succeeds in three of four (with one collision), while WM3 fails to reach the target in every run, instead entering a looping behavior that exhausts the time limit, although the flight remains collision-free. In the open-loop imagination test, where the model flies on hallucinated observations after a brief context window of 2.5 s, all models complete the traverse. These results confirm that the models that generalize well during SSL pretraining transfer reliably to the real world, whereas WM3, despite dominating the in-simulation policy evaluation, does not.